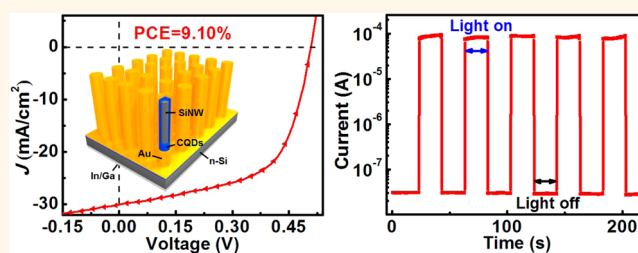


Core–Shell Heterojunction of Silicon Nanowire Arrays and Carbon Quantum Dots for Photovoltaic Devices and Self-Driven Photodetectors

Chao Xie,^{†,*} Biao Nie,[‡] Longhui Zeng,[‡] Feng-Xia Liang,[†] Ming-Zheng Wang,[‡] Linbao Luo,^{‡,*} Mei Feng,[§] Yongqiang Yu,[‡] Chun-Yan Wu,[‡] Yucheng Wu,^{†,*} and Shu-Hong Yu^{§,*}

[†]School of Materials Science and Engineering and [‡]School of Electronic Science and Applied Physics, Anhui Provincial Key Laboratory of Advanced Functional Materials and Devices, Hefei University of Technology, Hefei 230009, People's Republic of China and [§]Division of Nanomaterials and Chemistry, Hefei National Laboratory for Physical Sciences at Microscale, Collaborative Innovation Center of Suzhou Nano Science and Technology, Department of Chemistry, University of Science and Technology of China, Hefei 230026, People's Republic of China

ABSTRACT Silicon nanostructure-based solar cells have lately intrigued intensive interest because of their promising potential in next-generation solar energy conversion devices. Herein, we report a silicon nanowire (SiNW) array/carbon quantum dot (CQD) core–shell heterojunction photovoltaic device by directly coating Ag-assisted chemical-etched SiNW arrays with CQDs. The heterojunction with a barrier height of 0.75 eV exhibited excellent rectifying behavior with a rectification ratio of 10^3 at ± 0.8 V in the dark and power conversion efficiency (PCE) as high as 9.10% under AM 1.5G irradiation. It is believed that such a high PCE comes from the improved optical absorption as well as the optimized carrier transfer and collection capability. Furthermore, the heterojunction could function as a high-performance self-driven visible light photodetector operating in a wide switching wavelength with good stability, high sensitivity, and fast response speed. It is expected that the present SiNW array/CQD core–shell heterojunction device could find potential applications in future high-performance optoelectronic devices.



KEYWORDS: silicon nanowire array · carbon quantum dots · surface passivation · relative balance · barrier height

One-dimensional (1D) Si nanostructures with excellent electrical property and enhanced light absorption capability relative to their thin film or bulk counterparts have found wide-ranging applications in field-effect transistors,¹ biological and chemical sensors,^{2,3} logic circuits,⁴ photodetectors,⁵ etc. Among various 1D Si nanostructures (e.g., nanowires, nanoribbons, nanotubes), Si nanowires (SiNWs), in particular, vertically standing SiNW arrays with a strong light-trapping effect, have received increasing research interest due to their large interfacial area, fast charge transport,⁶ and the resulting high efficiency of charge collection by shortening the paths traveled by minority carriers.^{7,8} To date, a number of SiNW-array-based solar cells with high-energy conversion efficiency have been reported. For example, Lu *et al.* presented the fabrication of Si/PEDOT:PSS

core–shell nanowire array hybrid solar cells.⁹ The power conversion efficiency (PCE) of the solar cell was as high as 6.35% without any optimization. By using carbon thin film as an efficient surface passivation and modification layer for SiNWs, Wang *et al.* fabricated high-performance SiNW array photoelectrochemical solar cells with an impressive PCE of 10.86%.¹⁰

Nontoxic carbon quantum dots (CQDs), solely composed of chemically stable carbon, have attracted considerable attention due to their distinct difference from conventional semiconductor QDs. For example, unlike other II–VI semiconductor QDs (e.g., CdTe and CdSe), CQDs are usually produced in large scale by an alkali-assisted electrochemical etching approach.¹¹ This low-cost synthetic technique is more environmentally friendly than other solution-based methods. Furthermore, CQDs have demonstrated

* Address correspondence to
luolb@hfut.edu.cn,
ycwu@hfut.edu.cn,
shyu@ustc.edu.cn.

Received for review February 19, 2014
and accepted March 25, 2014.

Published online March 26, 2014
10.1021/nn501001j

© 2014 American Chemical Society

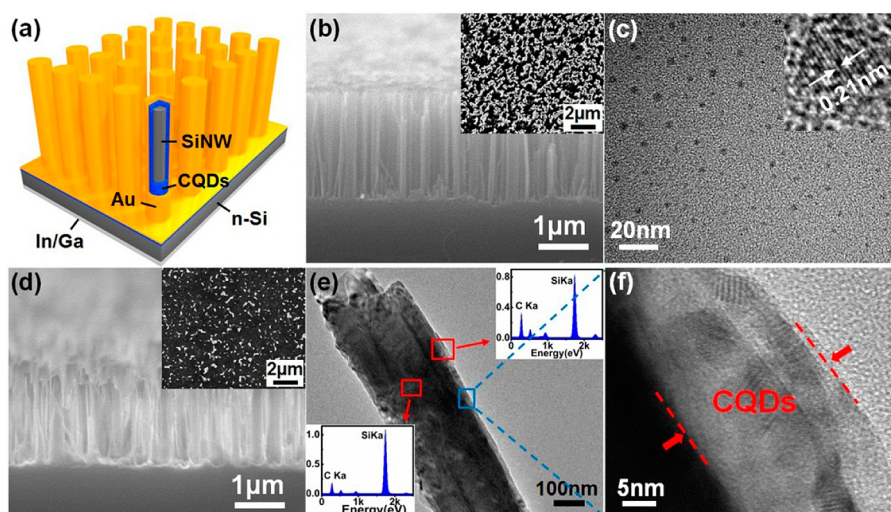


Figure 1. (a) Schematic illustration of the SiNW array/CQD heterojunction device. (b) SEM images of the as-prepared pristine SiNW arrays. (c) TEM image of the as-prepared CQDs; inset shows the HRTEM image of individual CQDs. (d) SEM images of the CH₃-terminated SiNW arrays coated with CQDs. (e, f) TEM images of individual SiNWs coated with CQDs. Insets in (e) are the EDS analysis on the CQD-coated SiNWs.

exceptional optical properties such as broad-band optical absorption and strong photoluminescence (PL) emission.¹² By this token, CQDs have been widely used to modify semiconductor nanoparticles, such as TiO₂, Fe₂O₃, and Ag₃PO₄, to substantially improve their photocatalytic abilities.^{13,14} In addition, it has been reported that TiO₂ nanotube arrays loaded with CQDs can function as an efficient photoanode for hydrogen generation,¹⁵ in which the hydrogen evolution rate was 14.1 μmol·h⁻¹ with long-term stability. Undeniably, the improvement of the above devices is mainly attributed to the widened optical absorption range with CQD functionalization. Enlightened by this, it is easy to come up with the idea of improving the SiNW-array-based photovoltaic device performance by attaching CQDs, which has been widely used in various QD-sensitized solar cells (QDSSCs).^{16,17}

To verify this concept, we assembled a SiNW array/CQD core–shell heterojunction by directly coating CQDs onto the NW surface. Electrical analysis of the core–shell nanostructures revealed excellent rectifying behavior with a rectification ratio of 10³ at ±0.8 V. Moreover, the heterojunction exhibited outstanding photovoltaic behavior, with PCE as high as 9.10%. By comparison of a planar counterpart and SiNW array devices without CQD coating, the reasons for the high photovoltaic performance of SiNW array/CQD heterojunctions were discussed. It was also found that the heterojunction could function as a photodetector under photoirradiation with good stability, high photosensitivity, as well as fast response speed in a wide range of switching frequencies.

RESULTS AND DISCUSSION

The proof-of-concept photovoltaic device (Figure 1a) was fabricated on n-type SiNW arrays with an average

length of ~2 μm and a diameter of hundreds of nanometers (Figure 1b). According to the statistical particle size distributions (Supporting Information, Figure S1a), the typical size of the CQDs is in the range of 2–6 nm, with an average diameter of ~4.5 nm. Further, the HRTEM image (inset in Figure 1c) indicates that the CQD is single-crystalline, and the *d*-spacing of the adjacent lattice planes for the QD is *ca.* 0.21 nm, corresponding to the (100) planes of graphite. Figure S1b depicts the reflectivity spectra of SiNW arrays before and after CH₃ termination (for comparison, the spectrum of planar Si was provided, as well). It can be seen that, compared with planar Si, pure SiNW arrays exhibit improved antireflection property in a wide spectrum. This phenomenon, normally known as the light-trapping effect, can be ascribed to light confinement within the nanostructures, which has been observed on ZnO NW arrays in previous work.¹⁸ Remarkably, the density of the NWs was somewhat reduced after CH₃ termination (Figure 1b,d). Such a reduction in density is highly favorable for the device performance because it can make the dispersion of CQDs more uniform during spin coating.^{19,20} Figure 1e shows a typical TEM image of a CQD-coated SiNW, showing that the SiNW is fully encapsulated by a continuous CQD film. From the HRTEM in Figure 1f, the thickness of the CQD shell is estimated to be ~23 nm, corresponding to ~5 layers of CQDs. In addition, the CQDs were closely packed on the surface of SiNW without any pinhole regions. Energy-dispersive X-ray spectroscopy (EDS) analysis on the CQD-coated SiNW is displayed in the insets of Figure 1e, indicating uniform coverage of CQDs on SiNWs. Furthermore, the UV–vis absorption spectrum together with the UPS analysis demonstrates that the as-prepared CQDs have a band gap of ~3.3 eV, a highest

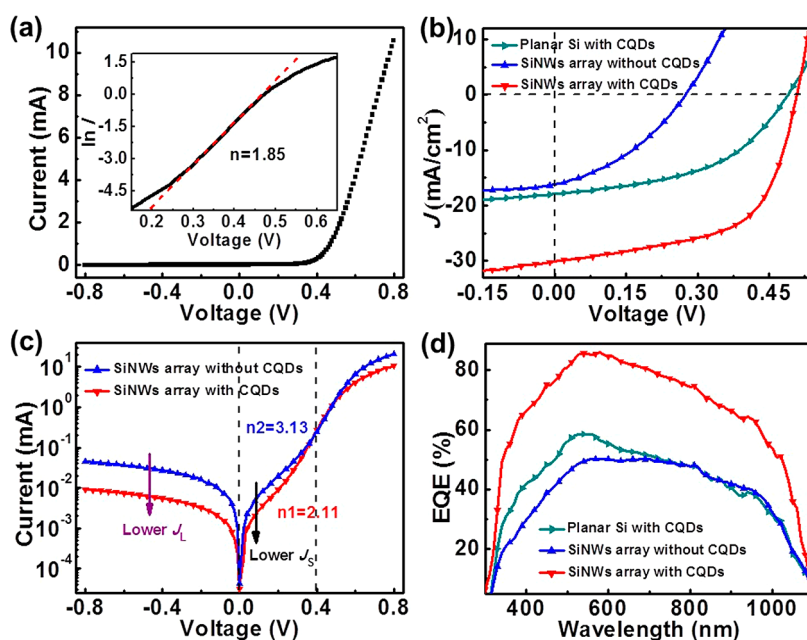


Figure 2. (a) Rectification characteristics of the optimal SiNW array/CQD heterojunction device in the dark. Inset: Plot of $\ln I$ versus voltage ($\ln I$ – V) shows ideality factor of the optimal SiNW array/CQD heterojunction device. Photovoltaic characteristics (b) and EQE spectra (d) of the optimal SiNW array/CQD heterojunction device and SiNW-array-based device without coating of CQDs as well as the CQD/planar Si heterojunction device for comparison. (c) Comparison of the I – V characteristics of the SiNW array devices without or with CQD coating.

occupied molecular orbital (HOMO) of -5.56 eV, and a lowest unoccupied molecular orbital (LUMO) of -2.26 eV (Supporting Information, Figure S2).

In order to improve the energy conversion efficiency by restricting the surface recombination activity, all chemically etched SiNW arrays were functionalized through the monolayer methyl termination method prior to device fabrication.²¹ Figure 2a shows a typical I – V curve of the SiNW array/CQD structure, from which excellent rectifying behavior can be easily observed. The rectification ratio is as high as 10^3 at ± 0.8 V in the dark, and a low turn-on voltage of ~ 0.45 V could be deduced at the forward bias direction. Based on the dark $\ln I$ versus voltage ($\ln I$ – V) curve (inset in Figure 2a), the diode ideality factor (n) is estimated to be 1.85. Furthermore, the barrier height (Φ_b) of the SiNW arrays/CQDs is calculated to be 0.75 eV (see Supporting Information), which is much larger than that of both graphene/n-Si (0.41 eV) and graphene/p-Si (0.45 eV) Schottky junctions.²²

The present SiNW array/CQD core–shell heterojunction offers two beneficial effects on photovoltaic device performance, that is, effective suppression of recombination activity and enhanced optical absorption. As mentioned above, the LUMO of CQDs is located at -2.26 eV, much higher than the conduction band minimum (E_c) of Si (-4.05 eV). Therefore, the resulting large E_c –LUMO offset (~ 1.8 eV) in the SiNW array/CQD device would constitute a large barrier for electron transport from SiNWs to the Au electrode (Figure 3d), leading to minimized recombination on the Au side by confining the electrons in SiNWs.

In other words, the CQD film could function as an electron blocking layer in the SiNW array/CQD device. According to a previous study, such reduction in recombination can lead to a low saturation current density (J_s) and a large V_{oc} (Figure 2c).²³ Figure S3a shows the optical absorption abilities of both CH_3 –SiNW arrays and CH_3 –SiNW arrays coated with a layer of CQDs. It is obvious that, in comparison with the former, the latter exhibits improved absorption in the near-UV light region.

Figure 2b plots the photovoltaic characteristics of various devices including SiNW array/CQD heterojunctions, planar Si/CQD heterojunctions, and SiNW array devices without CQD coating (Au/SiNW array Schottky junction). For comparison, the thickness of the CQD film in the first and second devices was kept at ~ 5 layers. Apparently, the SiNW array/CQD heterojunction exhibits the best photovoltaic performance, with an open-circuit voltage (V_{oc}), a short-circuit current density (J_{sc}), and a fill factor (FF) of 0.51 V, 30.09 mA cm^{-2} , and 0.593, respectively, yielding a PCE of 9.10%. This PCE is comparable to that of three-dimensional P3HT/Si nanopillar array hybrid solar cells (9.2%),¹⁹ as well as SiNW array/spiro-OMeTAD core–shell structure hybrid solar cells (9.70%),²⁴ but much higher than that of Si nanopillar array/PbS QD three-dimensional core–shell heterojunction solar cells (6.53%),²⁵ and SiNW array/PEDOT:PSS core–shell inorganic/organic hybrid solar cells (7.3%) (Table 1).²⁰ In comparison with the planar Si/CQD device, although the V_{oc} values of both devices are nearly the same, the J_{sc} of the planar Si/CQD device (17.93 mA cm^{-2}) is much smaller, only

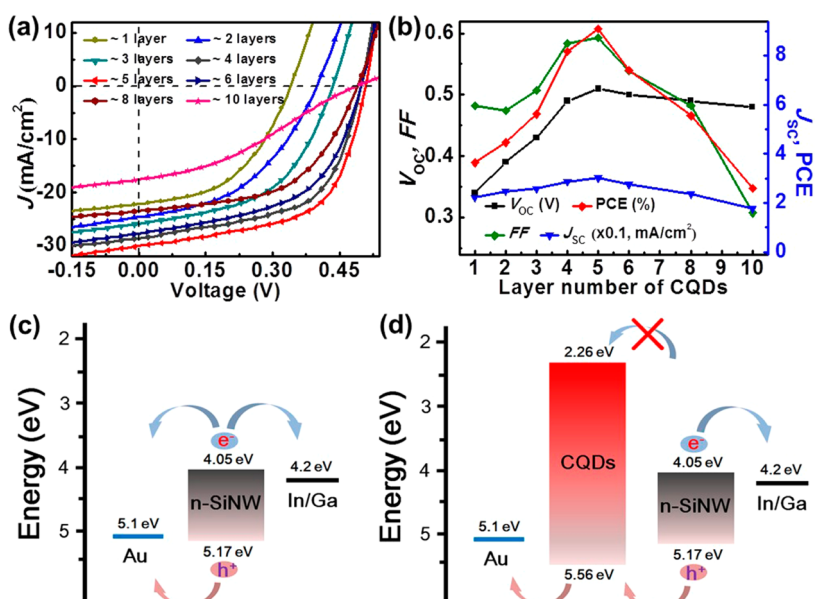


Figure 3. (a) Dependence of photovoltaic characteristics of SiNW array/CQD heterojunction devices on the thickness of CQDs. (b) Plots of V_{OC} , J_{SC} , FF, and PCE as functions of CQD layer number. Energy band diagrams of the Au/SiNW array Schottky junction (c) and the SiNW array/CQD heterojunction (d).

TABLE 1. Summary of the Photovoltaic Parameters of Several Typical Devices Studied in This Work

device structures	V_{OC} (V)	J_{SC} (mA cm ⁻²)	FF	PCE (%)
planar Si with 5 layers of CQDs	0.49	17.93	0.461	4.05
SiNW array without CQDs	0.27	16.22	0.362	1.58
SiNW array with 1 layer of CQDs	0.34	22.15	0.482	3.63
SiNW array with 5 layers of CQDs	0.51	30.09	0.593	9.10
SiNW array with 10 layers of CQDs	0.48	17.55	0.307	2.59

one-half that of the SiNW array/CQD device. It is believed that two factors are responsible for this comparatively high J_{SC} . First, owing to the strong light-trapping of SiNW arrays, the SiNW arrays exhibit enhanced light-harvesting capability relative to planar Si (Supporting Information, Figure S1b). As a result, more incident sunlight will be absorbed by SiNW arrays, giving rise to more photogenerated electron–hole pairs. Second, for the three-dimensional core–shell geometry of the SiNW array/CQD device, the increased interfacial area can fasten the charge transport, thus it will enable photogenerated minority carriers to travel a short distance to the heterojunction for efficient carrier collection. In fact, this supposition is partially verified by external quantum efficiency (EQE) analysis shown in Figure 2d, which shows a large value of above 60% over a wide wavelength range from 400 to 950 nm for SiNW array/CQD devices and a small value below 50% over the same wavelength range for planar Si/CQD devices.

With regard to the device without CQD coating, it displayed inferior photovoltaic performance with a PCE of only 1.58%, ~20% of that of the SiNW array/CQD device. Specifically, the V_{OC} , J_{SC} , as well as FF of

Au/SiNW array devices are much smaller than those of SiNW array/CQD devices. These low values for Au/SiNW array devices probably originate from the high recombination rate due to formation of metal–silicide in the Au/SiNW array¹⁹ and large current leakage (J_L) for Au–Si Schottky junction (Figure 2c).^{24,26} The barrier height of Au/SiNW array Schottky junction is estimated to be 0.61 eV, about 0.14 eV lower than that of the SiNW array/CQD heterojunction (0.75 eV) (see Supporting Information, eq 1 and eq 2). This low barrier height leads to large current leakage and small V_{OC} .²⁷ In addition, the relatively low FF can be ascribed to the decrease in shunt resistance in the circuit when the CQD layer is absent from the device. Based on the I – V curves (Supporting Information, Figure S3b), the ideality factors in the low voltage region ($V \leq 0.3$ – 0.5 V) can be estimated to be $n_1 = 2.11$ for the SiNW array/CQD junction and $n_2 = 3.13$ for the Au/SiNW array junction, suggesting a small shunt resistance and FF for the Au/SiNW array junction.^{28,29} To unveil the effect of CH₃ termination on device performance, two photovoltaic devices assembled from SiNW array/CQD heterojunctions and Au/SiNW array Schottky junctions without CH₃ termination were fabricated. Comparatively, these two devices exhibited inferior photovoltaic performance with PCEs of only 0.63% and 0.04%, respectively, much lower than that with CH₃ termination (Supporting Information, Figure S4). This result unambiguously confirms the important role of CH₃ termination in achieving highly efficient energy conversion.

It is worth noting that the photovoltaic performance of our core–shell structured solar cell is highly dependent on the film thickness of the shell layer. Figure 3a,b depicts the photovoltaic characteristics of the SiNW

array/CQD heterojunction as a function of CQD layer number. Obviously, compared to the device without CQD coating, the photovoltaic device parameters in terms of V_{OC} , J_{SC} , and FF increase immediately upon coating of monolayer CQDs on the SiNW arrays, yielding an increased PCE of 3.63%, which is more than twice that for the device without CQD coating (Table 1). As the layer number increased, the photovoltaic parameters increased correspondingly. The energy conversion efficiency approached a maximum value when the CQD layer reaches 5. Nevertheless, on the contrary, when the CQD layer continues to increase, the energy conversion efficiency begins to decrease. Understandably, the increasing device performance in thin layer CQDs (1–5 layers) is in part related to the increase in V_{OC} , as a result of decreased pinholes between the Au film electrode and SiNW array. It has been previously reported that pinholes are usually formed on the surface of SiNW arrays due to the nonuniform coating of CQDs.²⁵ In this case, Au could directly contact SiNWs in the pinhole to form a metal/Si Schottky junction and metal-silicide, which in turn leads to the reduction in V_{OC} , J_{SC} , and FF. Nonetheless, for devices with thick CQD layer coating (>5 layers), the pinholes nearly disappear in the thick layer, thus they can hardly influence the device performance any longer. For devices with a thick CQD layer, the device performance is mainly determined by two other factors, recombination and light-blocking effect, both of which can lead to reduced J_{SC} (recombination in the CQD layer becomes more serious due to poor electrical property; Supporting Information, Figure S5a). On the other hand, the thicker CQD layer would block a considerable amount of incident light from arriving at SiNWs (Supporting Information, Figure S5b). Moreover, the inferior conductivity of the thicker CQD layer would increase the series resistance in the circuit, which definitely decreases the FF.

To reveal how the CQD sizes will influence the photovoltaic characteristics, we further studied the photovoltaic characteristics of SiNW array/CQD heterojunctions with larger CQD sizes (average diameter of ~ 8 nm), as depicted in Figure S6. For comparison, the thickness of the CQD layer was kept the same as the device made of 4.5 nm CQDs. Apparently, this device shows inferior photovoltaic performance with V_{OC} , J_{SC} , and FF of 0.45 V, 27.71 mA cm⁻², and 0.581, respectively, yielding a PCE of 7.23%. The observed decrease in V_{OC} might be ascribed to the reduced barrier height of the heterojunction,¹² while the small J_{SC} might be related to the change of the electron/hole transport.

The charge separation and transport in SiNW array/CQD heterojunction solar cells could be understood from the energy band diagram in Figure 3d. Upon light irradiation, electron–hole pairs generated in Si would diffuse to the SiNW/CQD interface and then be separated by the strong built-in electric field. Electrons in

the conduction band of Si were preferentially collected by the bottom In/Ga electrode, while injection of electrons from the SiNW to the top Au electrode was prevented by the CQD layer due to the large E_C –LUMO offset. On the other hand, holes were readily injected into the HOMO level of the CQDs and collected by the Au electrode. This process results in the generation of photocurrent. In this device, the CQD layer can not only act as the hole transport layer but also serve as an electron-blocking layer for reducing the electron recombination at the top Au electrode.³⁰ The energy band diagram of the Au/SiNW array Schottky junction is also depicted in Figure 3c for comparison. It can be seen that, without the CQD electron-blocking layer, electrons generated in Si would have a large chance to diffuse toward Au and recombine at the electrode. This recombination process results in a large J_S and therefore a low V_{OC} of the photovoltaic device.²³ When the effect of both CQD layer and surface passivation is considered, it is expected that the performance of the SiNW array/CQD heterojunction solar cells could be further optimized by means of passivating the SiNW array surface with a more efficient approach, adjusting the band gap of CQDs, and increasing the conductivity of CQDs and so on.

Besides photovoltaic application, the SiNW array/CQD core–shell heterojunction could also function as a high-performance self-driven photodetector which can detect light irradiation without the need of exterior power supplies.³¹ Figure 4a illustrates the I – V curves of a representative SiNW array/CQD heterojunction device in semilogarithmic scale measured in the dark and under 600 nm light irradiation (100 mW cm⁻²), respectively. Significantly, the device exhibits pronounced response to the irradiation with a large photocurrent approaching 0.1 mA at zero voltage. The I_{light}/I_{dark} ratio (photosensitivity) is as high as approximately 3×10^3 . Further study of photoresponse characteristics of the device shown in Figure 4b reveals that the device can follow the fast-varying optical signal with good stability and reproducibility. Moreover, the responsivity (R), photoconductive gain (G), and detectivity (D^*) are estimated to be 353 mA W⁻¹, 0.693, and 3.79×10^9 cm Hz^{1/2} W⁻¹, respectively. It is noted that the R of this device is comparable to that of graphene/planar Si Schottky diode³² but far higher than the Cu/p-Si Schottky barrier-based near-infrared photodetector,³³ as well as the CdS/SiNW array radial heterojunction photodetector operated at zero bias.³⁴

Given that the response speed of a photodetector is essential for its practical application in light-wave communication and optical switches, the response speed of the SiNW array/CQD heterojunction photodetector was studied by using an optical chopper to generate the pulsed light with varied frequency from 0 to 2200 Hz at room temperature (inset in Figure 4d). It is interesting to note that our device exhibits high

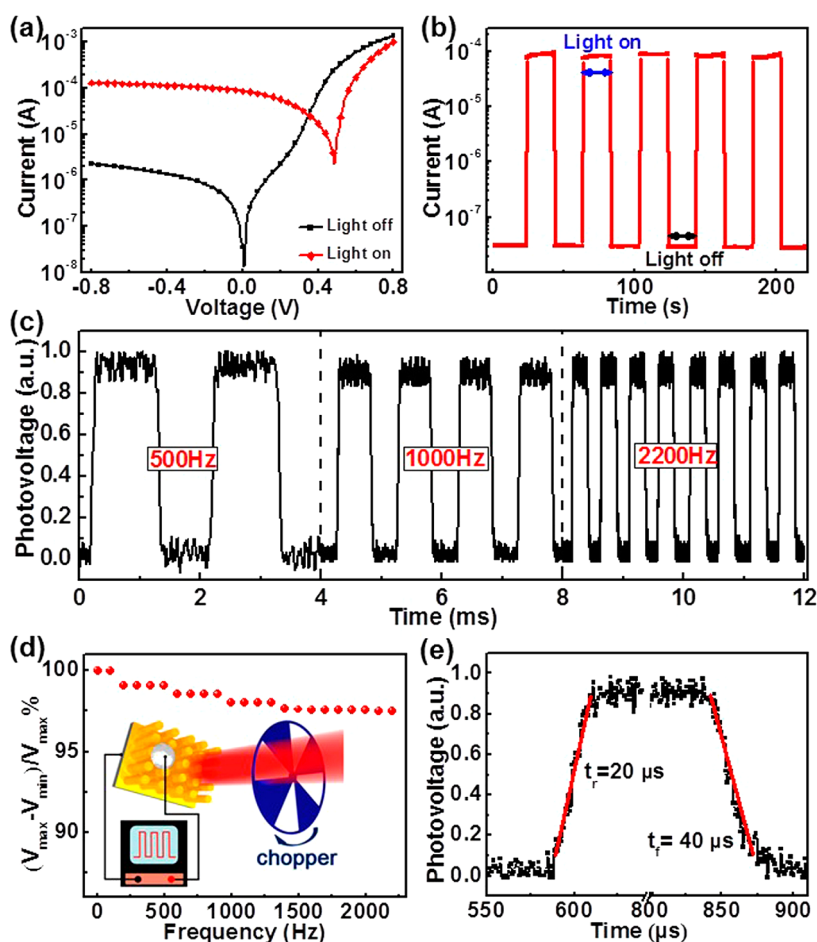


Figure 4. (a) I – V curves of the optimal SiNW array/CQD heterojunction device in the dark and under 600 nm photoirradiation. (b) Time response of the heterojunction device. (c) Response of the heterojunction device to the pulsed photoirradiation at frequencies of 500, 1000, and 2200 Hz. (d) Relative balance $(V_{\max} - V_{\min})/V_{\max}$ versus switching frequency. Inset shows the schematic illustration of the experimental setup for studying the time response of the SiNW array/CQD heterojunction device. (e) Rising and falling edges for estimated rise time and fall time.

sensitivity to all pulsed irradiation with frequencies from 500 to 2200 Hz, with excellent stability and reproducibility. Further study of the photovoltage as a function of chopping frequency reveals a slow relative balance $(V_{\max} - V_{\min})/V_{\max}$ decay (Figure 4d), and the relative balance remained larger than 96% even when the switching frequency increased to 2200 Hz. To the best of our knowledge, this value is the highest value ever reported. This result suggests that the SiNW array/CQD heterojunction photodetector can work well over a wide switching frequency range (Figure 4c), which is vitally important to monitor the ultrafast optical signal. Furthermore, from the magnified photoresponse curve in Figure 4e, the rise time and fall time could be estimated to be 20 and 40 μs , respectively. This response is much faster than our previous study on the photoresponse characteristics of p-CdTe nanoribbon/n-SiNW array heterojunction devices³⁵ and close to the commercial Si-based photodetector.³⁶ The fast response speed could be attributed to three aspects. First, the three-dimensional core–shell geometry of the photodetector could increase the SiNW/CQD

interfacial area and allows for the diffusion of the photogenerated carriers toward the depletion layer within a small distance, giving rise to quick separation and collection of the carriers. Second, the high-quality heterojunction formed between SiNW arrays and CQD can facilitate the effective and rapid separation of the photogenerated carriers as well. The above two reasons result in short rise time. Third, the efficient surface passivation by CH_3 termination can substantially suppress carrier trapping and releasing by reducing the SiNW surface's dangling bonds and surface states that can serve as carrier-trapping centers and reduce the rise and fall time.

Next, we investigated the air stability of the SiNW array/CQD heterojunction device by placing it under ambient conditions for 2 weeks without any encapsulation. It was found that the PCE of the SiNW array/CQD heterojunction device decreased by 14% to 7.82% (Figure S7). What is more, the $I_{\text{light}}/I_{\text{dark}}$ ratio is observed to slightly decrease from 3×10^3 to 2.7×10^3 . The gradual invalidation of CH_3 termination over time and the oxidation of the SiNW surface in air, which

increases the barrier for carrier transportation, might be the main reasons for the device performance degradation.

CONCLUSION

In summary, a new SiNW array/CQD core-shell heterojunction has been fabricated by a convenient cost-effective approach. The heterojunction with a barrier height of 0.75 eV exhibited pronounced rectifying behavior with a rectification ratio of 10^3 at ± 0.8 V and a PCE as high as 9.10%. It was found that the

thickness of the CQD layer played a key role in determining the device performance. Furthermore, the heterojunction device exhibits high sensitivity to 600 nm photoirradiation under zero bias with high photosensitivity ($\sim 3 \times 10^3$), large responsivity (353 mA W^{-1}), fast response speed (rise time = $20 \mu\text{s}$, fall time = $40 \mu\text{s}$). The above results suggest that this novel SiNW array/CQD heterojunction will open up new opportunities for future high-performance and low-cost optoelectronic devices.

METHODS

Preparation and Characterization of SiNW Arrays and CQDs. The vertical SiNW array was prepared by using a chemical etching approach.³⁷ The as-etched SiNW array was dipped into a diluted HNO_3 and HF solution to dissolve Ag and Si oxide on the surface, respectively. The SiNW array was then cleaned in deionized water several times and dried under a stream of nitrogen gas. The CQDs used in this work were synthesized by an electrochemical etching method.¹¹ After synthesis, the obtained solution was filtered with filter paper, and the resulting filtrate was centrifuged at 22 000 rpm for 30 min to screen off the large graphite particles. Finally, the CQDs were dispersed in ethanol solution for long time storage. The morphologies of the as-prepared SiNW arrays and CQDs were characterized by scanning electron microscopy (SEM, FEI/Quanta 200 FEG), transmission electron microscopy (TEM, FEI Tecnai G2 F20 S-TWIN), high-resolution transmission electron microscopy (HRTEM), and UV-vis absorption spectrum (Perkin-Elmer/Lambda 750) equipped with an integrating sphere. To study the energy levels of the CQDs, ultraviolet photoelectron spectroscopy (UPS, ULTRA DLD) analysis was carried out on a KRATOS-AXIS-165 spectrometer using Mg K α line.

Surface Passivation of SiNW Arrays. The hydrogen-terminated SiNW array (denoted as H-SiNW) was first obtained by immersing the as-prepared SiNW array into an aqueous HF solution (5 M) with gentle shaking for 10 min. The resulting sample was cleaned in deionized water for 1 min and dried by a stream of nitrogen gas. The methyl-terminated SiNW array (denoted as CH_3 -SiNW) was prepared by employing a two-step chlorination/alkylation process.^{38,39} The absorption spectra of as-prepared pristine SiNW arrays, CH_3 -terminated SiNW arrays, and planar Si were analyzed by a spectrometer (Perkin-Elmer/Lambda 750) equipped with an integrating sphere.

Conflict of Interest: The authors declare no competing financial interest.

Acknowledgment. This work was supported by National Key Basic Research Program of China (Grants 2012CB932400, 2013CB933500, 2010CB934700, 2013CB933900, 2014CB931800), the National Natural Science Foundation of China (Grants 51272062, 51172151, 21101051, 91022032, 91227103), the Chinese Academy of Sciences (Grant KJZD-EW-M01-1), the Fundamental Research Funds for the Central Universities (2012HGXC0003, 2013HGCH0012), and Major Research Plan of the National Natural Science Foundation of China (No. 91027021).

Supporting Information Available: Construction and evaluation of the heterojunction, calculation of the barrier height of the SiNW array/CQD heterojunction, the CQD size distribution histogram, reflectivity spectra of as-prepared pristine SiNW arrays and CH_3 -SiNW arrays and planar Si, UV-vis absorption spectrum and UPS spectrum of CQDs, absorption spectra of CH_3 -SiNW arrays and CH_3 -SiNW arrays with CQD coating, In I - V curves in low voltage region ($V \leq 0.3$ – 0.5 V) of SiNW array/CQD junction and Au/SiNW array junction. Photovoltaic characteristics of SiNW array/CQD heterojunction and Au/SiNW array Schottky junction; both devices are not CH_3 -passivated. I - V curve of ~ 5 layer CQD film based on a CQD thin film

transistor. Transmittance of the ~ 5 and ~ 10 layer CQD films on quartz glass. TEM image of CQDs with average diameter of 8 nm and the corresponding photovoltaic characteristics of SiNW array/CQD (8 nm) heterojunction devices. Photovoltaic characteristics and photodetecting properties of SiNW array/CQD heterojunctions over time. This material is available free of charge via the Internet at <http://pubs.acs.org>.

REFERENCES AND NOTES

- Cui, Y.; Zhong, Z. H.; Wang, D. L.; Wang, W. U.; Lieber, C. M. High Performance Silicon Nanowire Field Effect Transistors. *Nano Lett.* **2003**, *3*, 149–152.
- Cui, Y.; Wei, Q. Q.; Park, H. K.; Lieber, C. M. Nanowire Nanosensors for Highly Sensitive and Selective Detection of Biological and Chemical Species. *Science* **2001**, *293*, 1289–1292.
- Luo, L. B.; Jie, J. S.; Zhang, W. F.; He, Z. B.; Wang, J. X.; Yuan, G. D.; Zhang, W. J.; Wu, L. C. M.; Lee, S. T. Silicon Nanowire Sensors for Hg^{2+} and Cd^{2+} Ions. *Appl. Phys. Lett.* **2009**, *94*, 193101.
- Huang, Y.; Duan, X. F.; Cui, Y.; Lauhon, J.; Kim, K. H.; Lieber, C. M. Logic Gates and Computation from Assembled Nanowire Building Blocks. *Science* **2001**, *294*, 1313–1317.
- Xie, C.; Jie, J. S.; Nie, B.; Yan, T. X.; Li, Q.; Lv, P.; Li, F. Z.; Wang, M. Z.; Wu, C. Y.; Wang, L.; Luo, L. B. Schottky Solar Cells Based on Graphene Nanoribbon/Multiple Silicon Nanowires Junctions. *Appl. Phys. Lett.* **2012**, *100*, 193103.
- Weickert, J.; Dunbar, R. B.; Hesse, H. C.; Wiedemann, W.; Schmidt-Mende, L. Nanostructured Organic and Hybrid Solar Cells. *Adv. Mater.* **2011**, *23*, 1810–1828.
- Tian, B. Z.; Zheng, X. L.; Kempa, T. J.; Fang, Y.; Yu, N. F.; Yu, G. H.; Huang, J. L.; Liber, C. M. Coaxial Silicon Nanowires as Solar Cells and Nanoelectronic Power Sources. *Nature* **2007**, *449*, 885–889.
- Czaban, J. A.; Thompson, D. A.; LaPierre, R. R. GaAs Core-Shell Nanowires for Photovoltaic Applications. *Nano Lett.* **2009**, *9*, 148–154.
- Lu, W. H.; Wang, C. W.; Yue, W.; Chen, L. W. Si/PEDOT:PSS Core/Shell Nanowire Arrays for Efficient Hybrid Solar Cells. *Nanoscale* **2011**, *3*, 3631–3634.
- Wang, X.; Peng, K. Q.; Pan, X. J.; Chen, X.; Yang, Y.; Li, L.; Meng, X. M.; Zhang, W. J.; Lee, S. T. High-Performance Silicon Nanowire Array Photoelectrochemical Solar Cells through Surface Passivation and Modification. *Angew. Chem., Int. Ed.* **2011**, *50*, 9861–9865.
- Wang, F.; Zhang, Y. L.; Liu, Y.; Wang, X. F.; Shen, M. R.; Lee, S. T.; Kang, Z. H. Opto-Electronic Conversion Logic Behaviour through Dynamic Modulation of Electron/Energy Transfer States at the TiO_2 -Carbon Quantum Dot Interface. *Nanoscale* **2013**, *5*, 1831–1835.
- Li, H. T.; He, X. D.; Kang, Z. H.; Huang, H.; Liu, Y.; Liu, J. L.; Lian, S. Y.; Tsang, C. H. A.; Yang, X. B.; Lee, S. T. Water-Soluble Fluorescent Carbon Quantum Dots and Photocatalyst Design. *Angew. Chem., Int. Ed.* **2010**, *49*, 4430–4434.
- Zhang, H. C.; Ming, H.; Lian, S. Y.; Huang, H.; Li, H. T.; Zhang, L. L.; Liu, Y.; Kang, Z. H.; Lee, S. T. Fe_2O_3 /Carbon Quantum

- Dots Complex Photocatalysts and Their Enhanced Photocatalytic Activity under Visible Light. *Dalton Trans.* **2011**, 40, 10822–10825.
14. Zhang, H. C.; Huang, H.; Ming, H.; Li, H. T.; Zhang, L. L.; Liu, Y.; Kang, Z. H. Carbon Quantum Dots/Ag₃PO₄ Complex Photocatalysts with Enhanced Photocatalytic Activity and Stability under Visible Light. *J. Mater. Chem.* **2012**, 22, 10501–10506.
 15. Zhang, X.; Wang, F.; Huang, H.; Li, H. T.; Han, X.; Liu, Y.; Kang, Z. H. Carbon Quantum Dot Sensitized TiO₂ Nanotube Arrays for Photoelectrochemical Hydrogen Generation under Visible Light. *Nanoscale* **2013**, 5, 2274–2278.
 16. Lee, Y. L.; Lo, Y. S. Highly Efficient Quantum-Dot-Sensitized Solar Cell Based on Co-sensitization of CdS/CdSe. *Adv. Funct. Mater.* **2009**, 19, 604–609.
 17. Sun, W. T.; Yu, Y.; Pan, H. Y.; Gao, X. F.; Chen, Q.; Peng, L. M. CdS Quantum Dots Sensitized TiO₂ Nanotube-Array Photoelectrodes. *J. Am. Chem. Soc.* **2008**, 130, 1124–1128.
 18. Nie, B.; Hu, J. G.; Luo, L. B.; Xie, C.; Zeng, L. H.; Lv, P.; Li, F. Z.; Jie, J. S.; Feng, M.; Wu, C. Y.; Yu, Y. Q.; Yu, S. H. Monolayer Graphene Film on ZnO Nanorods Array for High-Performance Schottky Junction Ultraviolet Photodetectors. *Small* **2013**, 9, 2872–2879.
 19. Zhang, F. T.; Han, X. Y.; Lee, S. T.; Sun, B. Q. Heterojunction with Organic Thin Layer for Three Dimensional High Performance Hybrid Solar Cells. *J. Mater. Chem.* **2012**, 22, 5362–5368.
 20. Zhang, F. T.; Song, T.; Sun, B. Q. Conjugated Polymer-Silicon Nanowire Array Hybrid Schottky Diode for Solar Cell Application. *Nanotechnology* **2012**, 23, 194006.
 21. Zhang, X. Z.; Xie, C.; Jie, J. S.; Zhang, X. W.; Wu, Y. M.; Zhang, W. J. High-Efficiency Graphene/Si Nanoarray Schottky Junction Solar Cells via Surface Modification and Graphene Doping. *J. Mater. Chem. A* **2013**, 1, 6593–6601.
 22. Chen, C. C.; Aykol, M.; Chang, C. C.; Levi, A. F. J.; Cronin, S. B. Graphene-Silicon Schottky Diodes. *Nano Lett.* **2011**, 11, 1863–1867.
 23. Avasthi, S.; Lee, S.; Loo, Y. L.; Sturm, J. C. Role of Majority and Minority Carrier Barriers Silicon/Organic Hybrid Heterojunction Solar Cells. *Adv. Mater.* **2011**, 23, 5762–5766.
 24. Shen, X. J.; Sun, B. Q.; Liu, D.; Lee, S. T. Hybrid Heterojunction Solar Cell Based on Organic–Inorganic Silicon Nanowire Array Architecture. *J. Am. Chem. Soc.* **2011**, 133, 19408–19415.
 25. Song, T.; Zhang, F. T.; Lei, X. F.; Xu, Y. L.; Lee, S. T.; Sun, B. Q. Core–Shell Structured Photovoltaic Devices Based on PbS Quantum Dots and Silicon Nanopillar Arrays. *Nanoscale* **2012**, 4, 1336–1343.
 26. Brillson, L. J. The Structure and Properties of Metal–Semiconductor Interfaces. *Surf. Sci. Rep.* **1982**, 2, 123–326.
 27. Yang, H. T.; Shen, Y. D.; Edwall, D.; Miller, D. L.; Harris, J. S. Barrier Height Enhancement in Schottky-Barrier Solar Heterojunction Cells. *IEEE Trans. Electron Devices* **1980**, 27, 851–856.
 28. Jung, J. Y.; Um, H. D.; Jee, S. W.; Park, K. T.; Bang, J. H.; Lee, J. H. Optimal Design for Antireflective Si Nanowire Solar Cells. *Sol. Energy Mater. Sol. Cells* **2013**, 112, 84–90.
 29. Steim, R.; Choulis, S. A.; Schilinsky, P.; Brabec, C. J. Interface Modification for Highly Efficient Organic Photovoltaics. *Appl. Phys. Lett.* **2008**, 92, 093303.
 30. Xie, C.; Zhang, X. Z.; Wu, Y. M.; Zhang, X. J.; Zhang, X. W.; Wang, Y.; Zhang, W. J.; Gao, P.; Han, Y. Y.; Jie, J. S. Surface Passivation and Band Engineering: A Way toward High Efficiency Graphene-Planar Si Solar Cells. *J. Mater. Chem. A* **2013**, 1, 8567–8574.
 31. Wang, Z. L.; Wu, W. Z. Nanotechnology-Enabled Energy Harvesting for Self-Powered Micro-/Nanosystems. *Angew. Chem., Int. Ed.* **2012**, 51, 11700–11721.
 32. An, X. H.; Liu, F. Z.; Jung, Y. J.; Kar, S. Tunable Graphene-Silicon Heterojunctions for Ultrasensitive Photodetection. *Nano Lett.* **2013**, 13, 909–916.
 33. Casalino, M.; Sirlito, L.; Lodice, M.; Saffioti, N.; Gioffre, M.; Rendina, I.; Coppola, G. Cu/p-Si Schottky Barrier-Based Near Infrared Photodetector Integrated with a Silicon-on-Insulator Waveguide. *Appl. Phys. Lett.* **2010**, 96, 241112.
 34. Manna, S.; Das, S.; Mondal, S. P.; Singha, R.; Ray, S. K. High Efficiency Si/CdS Radial Nanowire Heterojunction Photodetectors Using Etched Si Nanowire Templates. *J. Phys. Chem. C* **2012**, 116, 7126–7133.
 35. Xie, C.; Luo, L. B.; Zeng, L. H.; Zhu, L.; Chen, J. J.; Nie, B.; Hu, J. G.; Li, Q.; Wu, C. Y.; Wang, L.; Jie, J. S. p-CdTe Nanoribbon/n-Silicon Nanowires Array Heterojunctions: Photovoltaic Devices and Zero-Power Photodetectors. *CrystEngComm* **2012**, 14, 7222–7228.
 36. Bae, J.; Kim, H.; Zhang, X. M.; Dang, C. H.; Zhang, Y.; Choi, Y. J.; Nurmikko, A.; Wang, Z. L. Si Nanowire Metal-Insulator-Semiconductor Photodetectors as Efficient Light Harvesters. *Nanotechnology* **2010**, 21, 095502.
 37. Peng, K. Q.; Fang, H.; Hu, J. J.; Wu, Y.; Zhu, J.; Yan, Y. J.; Lee, S. T. Metal-Particle-Induced, Highly Localized Site-Specific Etching of Si and Formation of Single-Crystalline Si Nanowires in Aqueous Fluoride Solution. *Chem.—Eur. J.* **2006**, 12, 7942–7947.
 38. Bansal, A.; Li, X. L.; Lauermann, I.; Lewis, N. S.; Yi, S. I.; Weinberg, W. H. Alkylation of Si Surfaces Using a Two-Step Halogenation/Grignard Route. *J. Am. Chem. Soc.* **1996**, 118, 7225–7226.
 39. Haick, H.; Hurley, P. T.; Hochbaum, A. I.; Yang, P. D.; Lewis, N. S. Electrical Characteristics and Chemical Stability of Non-oxidized, Methyl-Terminated Silicon Nanowires. *J. Am. Chem. Soc.* **2006**, 128, 8990–8991.